Development of a procedure to optimize the geometric and dynamic designs of assistive upper limb exoskeletons

Blanchet Laurent[1], Achiche Sofiane[1], Quentin Docquier[2], Paul Fisette[2], Raison Maxime[1]

[1]*Department of mechanical engineering, Polytechnique Montreal, Montreal, Canada*

[2]*Mechatronic, Electrical Energy, and Dynamic Systems (MEED), Institute of Mechanics, Materials and Civil Engineering (iMMC), Université catholique de Louvain, Louvain-la-Neuve, Belgium*

Email : laurent.blanchet@polymtl.ca, Phone : 450-931-0307

Keywords: Multibody, exoskeleton, optimization, optimal control, biomechanics, design

Abstract

The need for upper limb assistive and wearable exoskeletons is growing in various fields, e.g. either to support patients with neuromuscular disabilities or to reduce the effort strains on workers. These exoskeletons should reduce the efforts required by the user during functional tasks (dynamic consideration) and should fit the user's size (geometric consideration). This is a tedious task, due to the 3D human-exoskeleton interactions, and to the complex and interdependent selection of the power transmission characteristics, i.e. motors or passive elements. There are still few guidelines and few clear procedures to support geometric and dynamic syntheses of these exoskeletons.
The objective of this study is to develop a procedure for geometric and dynamic syntheses of assistive upper limb exoskeletons, to serve as a tool to optimize their design.

First, a geometric optimization of the exoskeleton dimensions enabled to maximize the kinematic loop closure and to avoid collisions with the body segments, while carrying out specific functional tasks. Secondly, through an optimal control problem, the dynamic characteristics of the exoskeleton were obtained by minimizing the user's joint torques for the functional tasks.

Closing the kinematic loops of the exoskeletons with optimized dimensions was achieved for all functional tasks, which was 10.8% more than with a visual identification of the dimensions. The resulting dynamic parameters could reduce the user's joint torque to less than 10.6% of the human-only simulations for nearly all joints and tasks.

These results showed that the geometric and dynamic synthesis procedures were successful. This is important, as it can enable the development of dedicated exoskeletons, such as lighter and smaller exoskeletons. The future perspectives will be to build an optimization framework, where the geometric and dynamic parameters could be optimized together, and to minimize the user's muscle forces instead of joint torques for specific design purposes.

1. Introduction

Exoskeleton devices are proliferating in rehabilitation, human-augmentation, and assistance fields. In rehabilitation, devices are used either to recover or develop motor skills for different types of patients. In this field, most devices are non-wearable [1, 2], as they use strong and heavy motors to provide functions such as haptic feedback [3] and precise motion for patient evaluation [4]. On their part, human-augmentation exoskeletons generally aim to provide the user with more strength [5, 6] for tasks such as lifting heavy objects or transporting heavy loads for certain distances [7]. The use of human-augmentation exoskeletons is of high interest for military and industrial applications; however, they generally rely on strong motors and bulky frames. Finally, wearable assistive exoskeletons are increasingly prevalent in research and they aim to ease pain and fatigue for industrial workers [8] and to assist patients with neuromuscular troubles that cause a lack of muscle force [9]. However, it should be noted that this prevalence is mainly true for the exoskeletons of lower limbs [10–12], while for the upper limbs, assistive and wearable devices are at their infancy stage [13].

A major obstacle for the development of wearable assistive exoskeletons, compared to rehabilitation or augmentation devices, is the tight constraints on the system size. To be comfortable to wear for a long period of time, the constraints on the overall size, and therefore on the sizing of dynamic actuators and geometric parameters make the design task more challenging [1].

To achieve a functional and optimal upper limbs exoskeleton design, the dynamics must be properly considered, where a first important concern is the appropriate sizing in terms of geometric size and power of the actuators.

A second major concern is the choice of the power transmission system. Some studies [14, 15] tended to develop fully passive exoskeletons to reduce weight and enhance portability. However, these ones were not able to assist the upper limb in many different tasks, as the elastic power transmission systems generally help the user for gravity affected movements only [16]. Therefore, for complex tasks such as opening a door, the user even tended to spend more effort with the exoskeleton [17, 18] than without it. To prevent such issues, some devices combined active and passive power transmissions [19], and one of the principal conclusions of these studies was that the passive mechanisms help lowering the size and power of the required motors [20].

To support the design of exoskeletons, different studies in multibody dynamics used models of kinematically constrained human limbs to an exoskeleton. These models were then optimized for various cost functions. For instance, the first optimized elements were often the geometric parameters, to find the optimal dimensions for the kinematic fit of the exoskeleton to the user [21] or to maximize force transmission from the exoskeleton to the user [22]. The second optimized elements were the dynamic parameters such as motor torques for active exoskeletons or passive elements characteristics such as springs for passive exoskeletons. In this case, the objective was to minimize the human effort such as joint torques [23] or powers [24], or muscle forces [25]. The dynamic optimizations can be formulated by non-linear problems using the computed generalized forces and torques from the inverse dynamics of the model for different tasks [25].

However, the inverse dynamics method does not consider the impact of the exoskeleton on the user's joint trajectories, as the generalized coordinates, velocities, and accelerations are not variables of the optimization. To overcome this challenge, one can use optimal control [26], where the optimization variables are the generalized positions, velocities and torques of the model, therefore the full interaction is considered. This approach was implemented in this study.

Despite the challenges of exoskeleton design related to the complex human-exoskeleton interaction and complex sizing and selection of power transmission systems, the literature has shown that there are very few guidelines and few clear procedures to support the geometric and dynamic syntheses of 3D wearable and assistive upper limb exoskeletons according to desired functional tasks.

Consequently, the objective of this study is to develop geometric and dynamic synthesis procedures, to serve as tools to design and personalize an upper limb exoskeleton for a given subject. This will be achieved through the execution of six specific functional tasks by one subject, such as eating with a spoon or opening a door, which were recorded in a state-of-the-art motion capture environment. Specific objectives are, first, to size the exoskeleton to fit the user for all the functional tasks and, secondly, to select the characteristics of the motors and passive elements to reduce the user effort for each task.

Highlights of this study

The main contribution of this research is the successful geometric and dynamic synthesis procedure for a 3D upper limb active and passive exoskeleton for 6 functional tasks. The specific highlights are that:

1. The developed geometric optimization framework enables the kinematic loop closure over all functional tasks, while avoiding collisions with the body segments.
2. The dynamic optimization framework reduces the torque required by the user's joints, while closely following the experimental trajectories of the functional tasks.
3. The dynamic optimization shows the importance of combining passive elements with motors, by enabling the size reduction of the required motors.

2. Methods

The global overview of the synthesis procedure of the upper limb exoskeleton is presented in Figure 1.

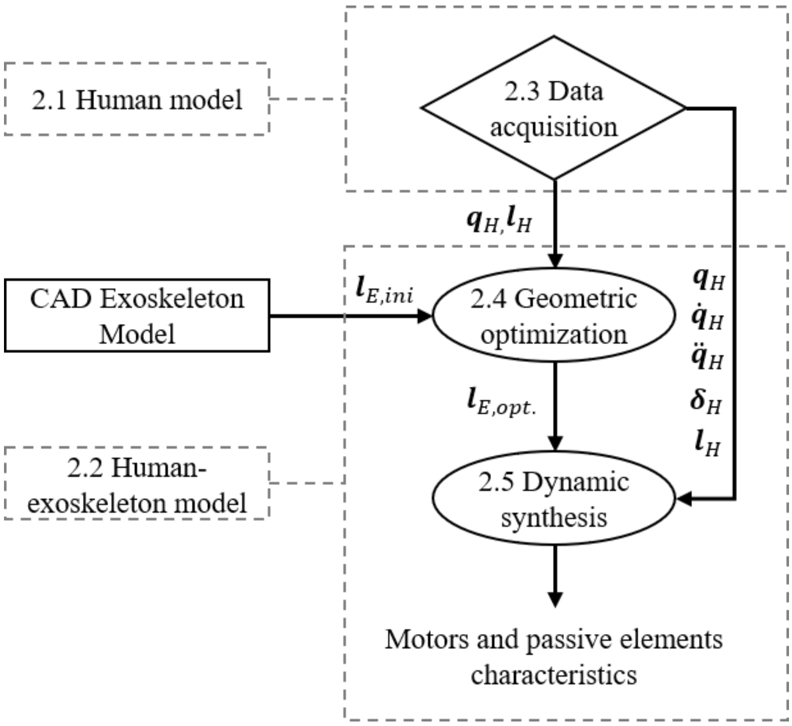

Figure 1. Synthesis procedure, including the functional tasks generalized positions, $\boldsymbol{q}_H$, velocities, $\dot{\boldsymbol{q}}_H$, and accelerations, $\ddot{\boldsymbol{q}}_H$, the subject body lengths $\boldsymbol{l}_H$ and the subject inertial parameters $\boldsymbol{\delta}_H$, the initial exoskeleton geometric parameters $\boldsymbol{l}_{E,ini}$ from the CAD exoskeleton model, the optimized exoskeleton geometric parameters $\boldsymbol{l}_{E,opt.}$

The first step of this procedure is the data acquisition (described in Section 2.3), which provides the functional tasks generalized positions, $\boldsymbol{q}_H$ [rad] or [m], velocities, $\dot{\boldsymbol{q}}_H$ $[\frac{\text{rad}}{\text{s}}]$

or $[\frac{\mathrm{m}}{\mathrm{s}}]$, and accelerations, $\ddot{\boldsymbol{q}}_H$ $[\frac{\mathrm{rad}}{\mathrm{s}^2}]$ or $[\frac{\mathrm{m}}{\mathrm{s}^2}]$, the subject body lengths $\boldsymbol{l}_H$ [m], and the body segment inertial parameters $\boldsymbol{\delta}_H$, i.e. mass [kg], center of mass [m], and moment of inertia [kgm^2]. The human model (Section 2.1), is used alone for this process. The geometric optimization and dynamic synthesis use the human-exoskeleton model (Section 2.2). The geometric optimization (Section 2.4) takes the $\boldsymbol{q}_H$, $\boldsymbol{l}_H$ provided by the data acquisition step, and the non-optimized exoskeleton geometric parameters $\boldsymbol{l}_{E,ini}$ [m] derived from its CAD model, to yield the optimized exoskeleton geometric parameters $\boldsymbol{l}_{E,opt.}$ [m] through a non-linear optimization. Finally, the dynamic synthesis (Section 2.5) takes the positions, $\boldsymbol{q}_H$, velocities, $\dot{\boldsymbol{q}}_H$, and accelerations, $\ddot{\boldsymbol{q}}_H$, the subject body lengths $\boldsymbol{l}_H$ and inertial parameters $\boldsymbol{\delta}_H$ from the data acquisition step and the $\boldsymbol{l}_{E,opt.}$ from the geometric optimization to provide the motors and passive elements characteristics through an optimal control problem, solved as a non-linear problem.

2.1 Human model

The full upper limb model shown in Figure 2 is based on the kinematics chain proposed by Laitenberger et al. [27], composed of the thorax, clavicle, scapula, humerus, ulna, radius, and hand. The thorax is considered as the moving base of the system, as it can move freely in relation to the ground. However, in this study, the moving base was fixed to simplify the optimization processes. As can be seen in Figure 2, the sternoclavicular (SC), acromioclavicular (AC) and glenohumeral (GH) joints are defined with spherical joints ($q_{H,7-9}, q_{H,10-12}, q_{H,13-15}$, respectively). The flexion/extension of the elbow joint is defined with a single revolute joint $q_{H,16}$, followed by a pronation/supination (PS) closed loop ($q_{H,17-21}$). This loop contains the humeroulnar (HU), radioulnar (RU), a virtual center of rotation (CoR) and the humeroradial (HR) joint which consists in a ball cut, i.e. a cut of ball joint, to close the loop. Finally, the radiocarpal joint at the hand is modeled with a universal joint ($q_{H,22-23}$).

The positions of the CoR and axis of rotation (AoR) for all joints were calculated using the symmetrical CoR estimation (SCoRE) and symmetrical axis of rotation approach (SARA) functional methods [28–30] respectively. These positions are represented by the body lengths $\boldsymbol{l}_H$. The segment inertial parameters, $\boldsymbol{\delta}_H$, i.e., mass, center of mass, and inertia were calculated by using the Yeadon anthropometric model [31].

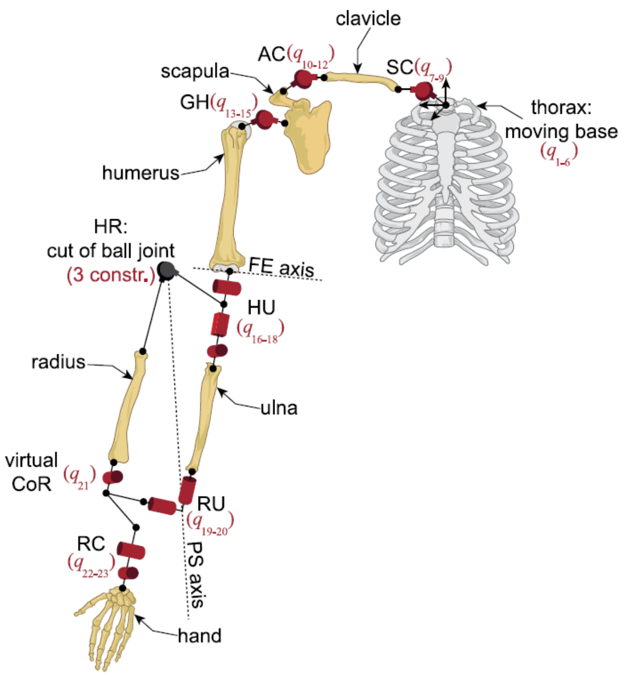

Figure 2. Kinematic chain of the human multibody model [27]. Sternoclavicular (SC) joint, $q_{H,7-9}$, acromioclavicular joint (AC), $q_{H,10-12}$, glenohumeral (GH) joint, $q_{H,13-15}$, humeroulnar (HU) joint, $q_{H,16-18}$, radioulnar (RU) joint, $q_{H,19-20}$, a virtual center of rotation (CoR), $q_{H,21}$, humeroradial (HR) joint, ball cut, and radiocarpal (RC) joint, $q_{H,22-23}$.

2.2 Human-Exoskeleton model

The exoskeleton model, based on [32] and shown in Figure 3, is a wearable and assistive exoskeleton, and its purpose is to help the user by compensating, in part or totally, the weight of his arm and in-hand objects in every day or work tasks.

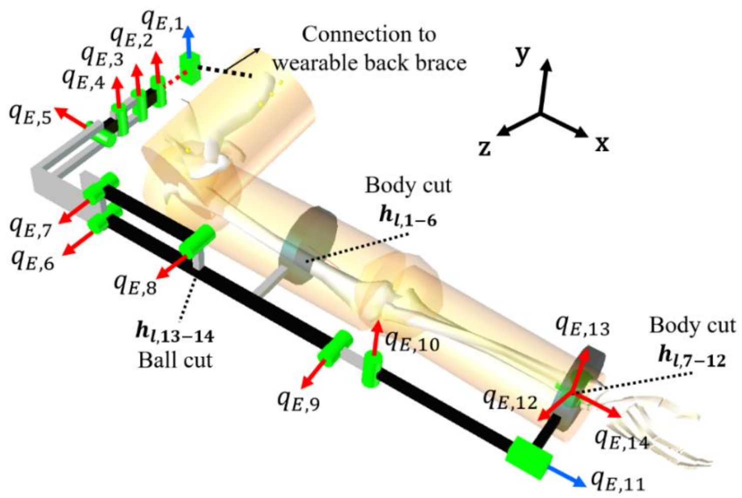

Figure 3. The exoskeleton model, with 14 generalized coordinates $\boldsymbol{q}_E$, 4 of which can be motorized and loaded with a torsion spring, $q_{E,5-6-9-14}$. The kinematic constraints by cutting the body represent the braces attached to the user's arm and the ball cut closes the four-bar loop mechanism.

The exoskeleton is designed to be attached to a wearable back brace. It is connected to the user's arm by braces at the upper arm and forearm, just before the wrist. These ones are described by the kinematics constraints of body cuts $h_{l,1-6}$ and $h_{l,7-12}$. The body cut constraints impose that the brace and arm possess a common point of attachment and that the orientation of the bodies must coincide at any time as described in [33].

In total, the exoskeleton is composed of four joints that could be motorized and eight additional passive joints. Additionally, each motorized joint can also be spring-loaded as a torsion spring can be inserted in the joint mechanism. To obtain a passive exoskeleton, the motorized joints can be compensated by the torsion springs only. The four-bar mechanism at the shoulder can be used to install a linear spring instead of a torsion spring in joint $q_{E,6}$, or to add an extra motor to assist the shoulder flexion extension movement.

In details, starting from the back fixation, there is one prismatic joint, $q_{E,1}$, and three redundant revolute joints, $q_{E,2-4}$. These passive joints help the exoskeleton adjust to the shoulder movements. Then there is the first motorized joint, $q_{E,5}$, which assists the abduction and abduction at the shoulder (S. AA). The four-bar mechanism follows up with three revolute joints, $q_{E,6-8}$ and a ball cut, $h_{l,13-14}$. Joints $q_{E,6}$ can be motorized to assist the shoulder flexion/extension (S. FE). The elbow joint $q_{E,9}$ can also be motorized to compensate for the flexion extension of the user's elbow (E. FE). To reach the wrist joint, four passive joints, $q_{E,10-11-12-13}$, let the exoskeleton adjust to the complex forearm pronation supination (F. PS) movement. Finally, at the wrist, there is the last motorized joint, $q_{E,14}$, which helps the F. PS movement. The inertial parameters, $\boldsymbol{\delta}_E$, i.e. mass, centers of masses and inertial parameters of the exoskeleton were determined with a CAD software.

The differential algebraic equation (DAE) system describing the human-exoskeleton closed loop system is given by Eq. 1 to Eq. 4:

$$\boldsymbol{M}(\boldsymbol{q},\boldsymbol{\delta})\ddot{\boldsymbol{q}} + \boldsymbol{c}(\boldsymbol{q},\dot{\boldsymbol{q}}) = \boldsymbol{Q}(\boldsymbol{q},\dot{\boldsymbol{q}}) + \boldsymbol{J}^T\boldsymbol{\lambda} \tag{1}$$

$$\boldsymbol{h}_l(\boldsymbol{q}) = 0 \tag{2}$$

$$\dot{\boldsymbol{h}}_l = \boldsymbol{J}(\boldsymbol{q})\dot{\boldsymbol{q}} = 0 \tag{3}$$

$$\ddot{\boldsymbol{h}}_l = \boldsymbol{J}(\boldsymbol{q})\ddot{\boldsymbol{q}} + \dot{\boldsymbol{J}}\dot{\boldsymbol{q}}(\boldsymbol{q},\dot{\boldsymbol{q}}) = 0 \tag{4}$$

where $\boldsymbol{q} = [\boldsymbol{q}_H\ \boldsymbol{q}_E]$, $\dot{\boldsymbol{q}} = [\dot{\boldsymbol{q}}_H\ \dot{\boldsymbol{q}}_E]$, $\ddot{\boldsymbol{q}} = [\ddot{\boldsymbol{q}}_H\ \ddot{\boldsymbol{q}}_E]$ are the complete generalized positions, velocities and accelerations, respectively, $\boldsymbol{\delta} = [\boldsymbol{\delta}_H\ \boldsymbol{\delta}_E]$ corresponds to the dynamic parameters of the system (body masses, centers of mass, inertias), $\boldsymbol{M}$ is the generalized mass matrix, $\boldsymbol{c}$ is the non-linear vector containing the external, gravity, centrifugal and gyroscopic forces, $\boldsymbol{Q}$ [Nm] or [N] is the generalized forces or torques vector that can be separated as $\boldsymbol{Q}_H$ and $\boldsymbol{Q}_E$, respectively, in the human and exoskeleton joints, $\boldsymbol{h}_l$ are the loop closure geometrical constraints, $\boldsymbol{J}$ is the Jacobian matrix of the system, $\dot{\boldsymbol{J}}\dot{\boldsymbol{q}}$ is the quadratic term of the constraints at acceleration level and $\boldsymbol{\lambda}$ represents the Lagrange multipliers associated with the constraints. As mentioned in the previous sections, $\boldsymbol{q}$ ($\dot{\boldsymbol{q}}$ or $\ddot{\boldsymbol{q}}$) can be grouped in $\boldsymbol{q_H}$ the generalized coordinates of the human, which corresponds to $\boldsymbol{q}_u$ the independent generalized coordinates, $\boldsymbol{q}_{\boldsymbol{H},v}$ the dependent generalized coordinates of the human, $\boldsymbol{q_E}$ the exoskeleton generalized coordinates, and finally the global dependent generalized coordinates $\boldsymbol{q}_v = [\boldsymbol{q}_{\boldsymbol{H},v}\ \boldsymbol{q_E}]$. All models and all symbolic equations were generated using ROBOTRAN Multibody dynamics software [34] based on recursive formalisms for kinematics and dynamics [33].

2.3 Data acquisition

To develop and illustrate the development of geometric and dynamic synthesis procedures, data from one healthy subject (Age: 25, Mass: 90 kg, Height: 1.93 m) were acquired by using the set of reflective markers, as proposed in [27]. The study was approved by the institutional ethical committee, and the participant gave his informed consent. This set ensured at least 4 markers per body for redundancy and technical markers to minimize soft tissue artefacts. The 3D markers trajectories were measured at 100 Hz by a motion-capture system composed of 12 cameras (T40S, Vicon-Oxford, UK). A total of 6 different functional tasks were executed and selected from the study by Rosen et al. [35]. The tasks, described in Table 1, were chosen to mimic activities of daily life and to ensure a broad range of amplitudes for each joint. The data for the SCoRE and SARA methods were also acquired to find the CoR and AoR of the subject. The user's relative coordinates $\boldsymbol{q}_H$ were computed by the kinematics identification process described in [36]. This process minimizes the difference between the experimental 3D marker coordinates and the marker coordinates obtained by the forward kinematics function of the multibody system.

Table 1 - Recorded functional tasks and their abbreviations.

Functional tasks	Abbreviations
Eat with a spoon	ES
Arm frontal reach	AR
Arm reach right to left	RL
Open a door	OD
Zip your coat	ZC
Comb your hair	CH

2.4 Geometric optimization

The goal of the geometric optimization is to maximize the *"exoskeleton fit"* to the user while doing functional tasks. This *"exoskeleton fit"* can be defined by the combination of three elements:

1. The loop constraints $\boldsymbol{h}_l(\boldsymbol{q}, \boldsymbol{l})$ between the arm and the exoskeleton must be satisfied, where $\boldsymbol{q}$ are the relative coordinates for the combined human-exoskeleton model and $\boldsymbol{l}$ are the combined human and exoskeleton dimensions;
2. There are no collisions between the arm and the exoskeleton during the execution of the functional tasks;
3. The exoskeleton is closely fit to the user to:
   - lower the size and weight of the exoskeleton, to increase the user's comfort;
   - reduce the lever arms across the exoskeleton bodies, although this was not studied in this research.

To combine all functional tasks in this study, each task was optimized one by one, and the results were used to provide a better initial guess for the second optimization, where all the functional tasks were optimized simultaneously. This allowed for the exoskeleton to be sized to the user for all tasks.

2.4.1 Loop closure

Generally, to solve the loop constraints $\boldsymbol{h}_l$ presented in Eq. 2, a Newton-Raphson algorithm is used [33]. However, if the constraints cannot be satisfied, i.e., the MBS cannot achieve loop closure, the result of the Newton-Raphson procedure is an inconsistent system, far from the loop closure [37]. In this study, and for exoskeletons in general, with the uncertainties coming from the user's skin movement, the precision of the exoskeleton dimensions or the 3D marker trajectories errors, constraints $\boldsymbol{h}_l$ may not always reach a solution. Instead, following the method proposed by [37], the loop constraints were minimized (Eq. 5), as this provides a solution even if the loop cannot be closed by the Newton-Raphson method. However, if the system can be closed, $\boldsymbol{h}_l$ will be equal to 0, as with Newton-Raphson.

$$\min_{\boldsymbol{l}_E, \boldsymbol{q}_v} L_C = \frac{1}{2} \boldsymbol{h}_l(\boldsymbol{q}, \boldsymbol{l})^T \boldsymbol{h}_l(\boldsymbol{q}, \boldsymbol{l}) \tag{5}$$

The independent relative coordinates $\boldsymbol{q}_u$ were not considered as optimization variables here as they describe the displacement of the user's arm in functional tasks. The optimization process makes vary the dependent relative coordinates $\boldsymbol{q}_v$, which are the exoskeleton joints $\boldsymbol{q}_E$, and the forearm loop dependent coordinates $\boldsymbol{q}_{H,v}$. The exoskeleton lengths, $\boldsymbol{l}_E$, are also variables of the optimization.

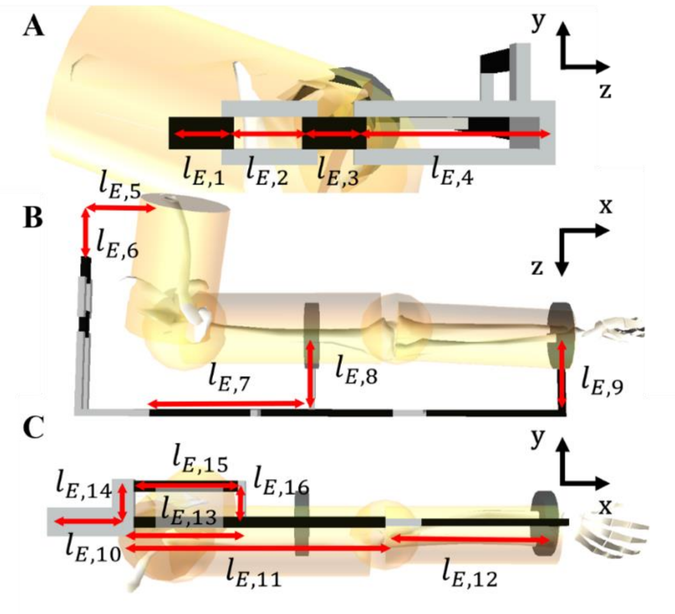

Figure 4. Exoskeleton optimized dimensions. A. Rear view of the human-exoskeleton model showing dimensions $l_{E,1-4}$. B. Top view of the human-exoskeleton model showing dimensions $l_{E,5-9}$. C. Side view of the human-exoskeleton model showing dimensions $l_{E,10-16}$.

Figure 4 shows the optimized exoskeleton dimensions. Dimensions $l_{E,1-6,10}$ help to avoid collisions with the shoulder; dimension $l_{E,7-8}$ aim to help reach the arm brace; dimension $l_{E,11}$ aims to help reach the elbow joint and dimension $l_{E,9,12}$ aim to help reach the wrist brace. Finally, dimensions $l_{E,13-16}$ are used to size the four-bar mechanism, so that it does not interfere with the rest of the exoskeleton.

2.4.2 Collision avoidance

For the collision avoidance, the method was based on [38], where the human body is described as a succession of cylinders and spheres with dimensions according to the Yeadon anthropometric model [31], and describing each exoskeleton bodies as cylinders of radius r_{body} [m] equal to the biggest dimension of the corresponding body.

This ensures that the volume of the cylinder is bigger than the real body. Then the lowest distances $\boldsymbol{d_c}$ [m] between the human shapes and exoskeleton shapes were used as constraints, $\boldsymbol{d_c} > 0$.

2.4.3 Minimization of the exoskeleton size

To reduce the exoskeleton size, the distances between the exoskeleton body points and the chosen human body points were minimized using Eq. 6. The set of minimized distance $\boldsymbol{d}$ [m] is exoskeleton dependent and should address the most important distances. In this case, the distance between the exoskeleton and the human body is mostly important around the shoulder and behind the user as the exoskeleton tends to be far from the shoulder joints to avoid collisions. Figure 5 shows the chosen points, SC, AC2, and AC. Moreover, according to the exoskeleton kinematic chain and loop closure constraints, d_7 generally corresponds to the distance between the exoskeleton and the human arm, $l_{E,8}$ and $l_{E,9}$, for all bodies after joint $q_{E,6}$.

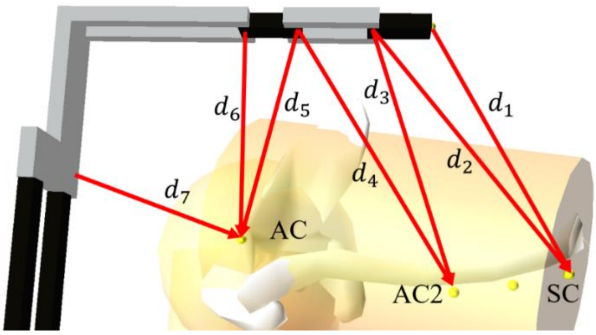

Figure 5. Close up of a top view of the human-exoskeleton model showing distances d_{1-7}.

The minimization of these distances is then, as shown in Eq. 6:

$$\min_{\boldsymbol{l},\boldsymbol{q}_v} D = \sum_{i=1}^{n} d_i(\boldsymbol{q},\boldsymbol{l}) \tag{6}$$

where d_i is the distance between each point i , and n is equal to the number of distances, here 7.

2.4.4 Optimization framework

The optimization framework combining the three elements of the *exoskeleton fit* to the user is described by the cost function (Eq. 7) composed of weighted Eqs. 5, L_C, and 6, D, for all the recorded functional tasks $\boldsymbol{q}_{u,k}$ recorded for the functional tasks:

$$\min_{\boldsymbol{l}_E,\boldsymbol{q}_v} \sum_{\boldsymbol{q}_{u,1}}^{\boldsymbol{q}_{u,j}} \left[p_{loop}\, L_C + p_{dist}\, D\right] \tag{7}$$

where p_{loop} and p_{dist} are respectively weights for each part of the cost function. $j = 1\ to\ 6$ is the index of the functional task. As the loop closure is of the utmost most importance in this optimization process, p_{loop} was chosen to be $1e^4$. This is a realistic choice, as Newton-Raphson loop closure is usually achieved at $1e^{-6}$ in this problem. p_{dist} was chosen to be 1.

The constraints for this framework were the physical boundaries on the exoskeleton generalized coordinates, to ensure realistic mechanism movements. Furthermore, on top of the collision avoidance constraints, more constraints were added to ensure the four-bar parallelism, and to keep the same distance between exoskeleton and the user's arm after the shoulder joint.

Initial values for the dimensions of the exoskeleton bodies $\boldsymbol{l}_{E,ini}$ were identified visually in the exoskeleton CAD model, and initial values for the $\boldsymbol{q}_v$ were obtained by the kinematics of the non-optimized exoskeleton while executing the functional tasks.

2.5 Dynamic synthesis

The global objective of the dynamic synthesis is to determine the required motors and passive elements characteristics to design the exoskeleton for the functional tasks and the user. An important part of this synthesis is the dynamic optimization problem described by Sections 2.5.1 to 2.5.3. Its objective is to find the adequate exoskeleton generalized joint torques $\boldsymbol{Q}_E$ to assist and minimize the user's generalized joint torques $\boldsymbol{Q}_H$. Finally, Section 2.5.4 presents the dynamic synthesis procedure.

2.5.1 Exoskeleton generalized joint torques evaluation

The equivalent of torsion springs is used as passive elements as they are easy to model with the linear Hooke's Law. To evaluate the motors and springs characteristics, $\boldsymbol{Q}_E$ must be divided in two parts, $\boldsymbol{Q}_M$ for the torque produced by the motors and $\boldsymbol{Q}_S$ for spring induced torques. The latter can be written with Hooke's law for a torsion spring, as follows, Eq. 8:

$$Q_{S,i} = k_i(q_{E,i} - q_{0,i}) \tag{8}$$

where k_i is the stiffness constant $[\frac{\mathrm{Nm}}{\mathrm{rad}}]$ of the spring i, and $q_{0,i}$ is its neutral position [rad]. These parameters will be variables of the optimization process. Then, the full joint torque can be computed as follows, Eq. 9:

$$Q_{E,i} = Q_{M,i} + Q_{S,i} \tag{9}$$

2.5.2 Optimal control problem

The dynamic optimization taking the full human-exoskeleton interaction into account was formulated as DAE constrained optimal control problem (OCP) with cost functional J, and can be written as follows [39, 40]:

$$\min_{x(t),u(t)} J = \Phi(\boldsymbol{x}(t_0), t_0) + \int_{t_0}^{t_f} L(\boldsymbol{x}(t), \boldsymbol{u}(t), t)dt \tag{10}$$

where $\boldsymbol{x}(t)$ is the state vector, $\boldsymbol{u}(t)$ is the control vector, t_0 is the initial time, t_f the final time, Φ is the scalar terminal weighting function, and L the scalar function. Eq. 10 is subject to Eqs. 11 to 14:

$$\boldsymbol{x}_0 = \boldsymbol{x}(t_0) \tag{11}$$

$$F(\dot{\boldsymbol{x}}(t), \boldsymbol{x}(t), \boldsymbol{u}(t), t) = 0 \tag{12}$$

$$g(\boldsymbol{x}(t), \boldsymbol{u}(t), t) \geq 0 \tag{13}$$

$$\varphi\left(\boldsymbol{x}(t_f)\right) = 0 \tag{14}$$

where, $\boldsymbol{x}_0$ is the fixed initial state, F are the dynamic equations of the system described by Eqs.1 to 4, g are the inequality constraints on the control and state variables, and φ denotes the terminal state constraints. As a forward dynamic formulation of the dynamics was used, the state vector was defined as $\boldsymbol{x}(t) = [\dot{\boldsymbol{q}}_u \ \boldsymbol{q}_u]$, and the control vector as $\boldsymbol{u}(t) = [\boldsymbol{Q}_H \ \boldsymbol{Q}_M \ \boldsymbol{k} \ \ \boldsymbol{q}_{\boldsymbol{0}}]$.

2.5.3 Non-linear optimization process

To solve this OCP, a direct collocation approach was used, which allows simultaneous simulation and optimization [41]. The problem was built in CasADi symbolic framework [42]. In this method, the state vector $\boldsymbol{x}(t)$, and control vector $\boldsymbol{u}(t)$ were discretized on a fine grid of collocation points and then approximated by using Lagrange polynomials and piecewise constant function respectively. Time integration was approximated with quadrature formula for the same collocation points [43]. Continuity constraints ensure smoothness between the state intervals. We used a *Radau* time grid, as it provides a collocation point at the start and end of every state [44].

The first part of the cost function minimized the normalized user's joint torques, as follows, Eq. 15:

$$T = \min_{\boldsymbol{Q_H},\boldsymbol{Q_M},\boldsymbol{k},\boldsymbol{q_0},\dot{\boldsymbol{q}}_u\ \boldsymbol{q}_u} \sum_{j=1}^{N} \int_{t_j}^{t_{j+1}} \sum_{i=1}^{n} \frac{Q_{H,i,j} \cdot Q_{H,i,j}}{\max\left(Q_{H,i,exp.}\right)^2} dt \tag{15}$$

where n was the number of independent actuated joints of the human, max ($Q_{H,i,exp.}$) was the maximum experimental torque for joint i, t_j was the time of collocation interval j and N was the number of collocation intervals. As the goal of this process was the design of a user-centered exoskeleton device, the trajectory of the user's joints was important to produce feasible and intuitive movements. To do this, the error between the experimental data and the simulated generalized positions was minimized by using Eq. 16:

$$P = \min_{\boldsymbol{Q_H},\boldsymbol{Q_M},\boldsymbol{k},\boldsymbol{q_0},\dot{\boldsymbol{q}}_u\ \boldsymbol{q}_u} \sum_{j=1}^{N} \int_{t_j}^{t_{j+1}} \sum_{i=1}^{n} (\boldsymbol{q}_{u,j,exp.} - \boldsymbol{q}_{u,j})^2 dt \tag{16}$$

The whole cost function was then Eq. 15 + Eq. 16, leading to the following minimization Eq. 17:

$$\min_{\boldsymbol{Q_H},\boldsymbol{Q_M},\boldsymbol{k},\boldsymbol{q_0},\dot{\boldsymbol{q}}_u\ \boldsymbol{q}_u} T + P \tag{17}$$

The first set of constraints is described by the collocation continuity constraints between the state intervals as explained above. For the path constraints on the generalized positions, articular limits were considered for the user's joints [45], and kinematic limits in respect to the CAD model for the exoskeleton joints. No path constraints were used on the user's joint torques, as the minimization of the trajectory error ensured realistic torques and movements. However, these could easily be added as the maximum joint torques for each joint. For the exoskeleton dynamic passive elements, i.e. torsion springs, parameters $\boldsymbol{k}$ and $\boldsymbol{q_0}$, an equality constraint was used as they must be constant for the whole trajectory.

Eq. 9 describes the exoskeleton joint torques evaluation according to the use of either passive elements, or motors, or both. For the motor parameters, the torque and speed can be limited by their winding curve. Winding curves for several motors were approximated by a linear relationship between the motor maximum torque at quasi no velocity state, which is generally lower than the stall torque and the maximum continuous torque at the maximum continuous velocity of the motor. Continuous torques could not always be found therefore their value was safely put to 0 Nm. The motor parameters for three manufacturers, Herkulex (HKX), Dynamixel (DMX), and

Maxon (MAX), each with several motors, are shown in Appendix A (Table 3) and were generally found on the datasheets listed on the Websites of the manufacturers. As an example, Figure 6 shows the intermediary result of the motor winding constraints on the shoulder joint. The motor used in this evaluation is the DMX XH540. Its limits are reached in the top right corner when used without a spring, but when used with a spring, the motor no longer reaches its torque limits.

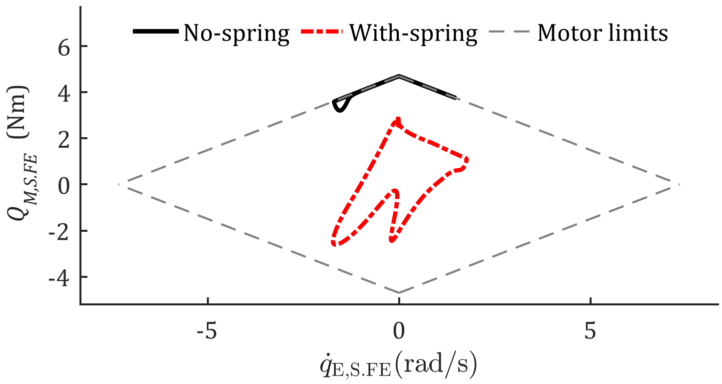

Figure 6. The exoskeleton motor (DMX XH540) torque at the shoulder joint compared with the motor speed. The no-spring optimization reaches the winding limits of the motor while the with-spring optimization is within the motor limits.

To help the solver, each experimental trajectory was divided by groups of collocation intervals which were then combined in a final optimization to obtain the full trajectory. This was done for all OCP evaluations. For each group of intervals, the experimental data kinematics and inverse dynamics results were used as initial guess for $\boldsymbol{Q}_H$, $\dot{\boldsymbol{q}}_u$ and $\boldsymbol{q}_u$. Additionally, $\boldsymbol{Q_M}, \boldsymbol{k}$ and $\boldsymbol{q_0}$ are set to zero. Results for human-only OCP trajectories and torques are shown in Appendix B.

2.5.4 Dynamic synthesis procedure

To optimize the exoskeleton design for the six functional tasks, we follow the procedure presented in Figure 7, where n_T, n_J and n_M are respectively the current evaluated task, joint and motor, N_T, N_J and N_M are the quantity of tasks, joints and motors, here, 6, 4, and 9. Q_{H,n_J} and Q_{M,n_J} are, respectively, the user's joint torque and exoskeleton joint torque at the evaluated joint n_J. The joints n_J are $q_{H,13,14,16\ and\ 19}$ from Figure 2 for the user's joints and $q_{E,5,6,9\ and\ 14}$ from Figure 3 for the exoskeleton. The 4 joints are for the S. AA, S. FE, E. FE and F. PS movements. $Q_{H,n_J.HO}$ is the user's joint torque for the human-only simulation.

As seen in Figure 7, the process starts with the first task and the most distal joint, F. PS, as the motor selection for n_J affects n_{J-1}, n_{J-2}, etc. Therefore, this process can be seen as a backward recursive joint sizing. Then, the dynamic optimization is performed with $n_M = 1$ the smallest motor, here HKX 101. The most important element of the process is the final decision block, where 2 alternative conditions enable to accept the choice of motor for the joint and task:

- First condition: The ratio between the RMS value of user's joint torque while wearing the exoskeleton, and the RMS value of the user's joint torque without exoskeleton, is lower than the condition threshold C, where C is chosen between 0 and 1 by the exoskeleton designers. A 0 value means the user does not need to produce torque and a 1 value means the user needs to produce all the torque. Hereafter, threshold C will be defined as the *user torque ratio.*
- Second condition: The motor torque, Q_{M,n_J}, is within the motor winding limits for the whole trajectory.

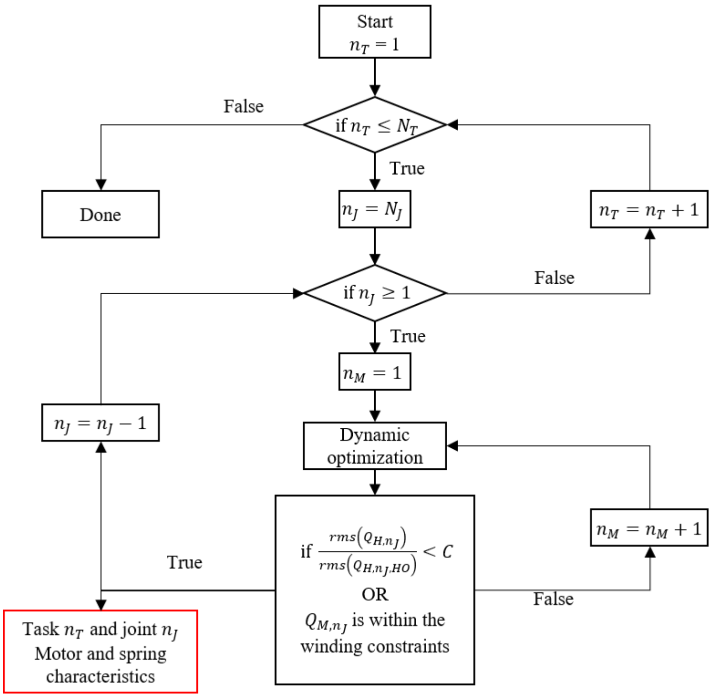

Figure 7. Dynamic synthesis procedure. n_T, n_J and n_M are respectively the current evaluated task, joint and motor. N_T, N_J and N_M are the quantity of task, joint and motor. Q_{H,n_J} and Q_{M,n_J} are, respectively, the user's joint torque and exoskeleton joint torque at the evaluated joint n_J. $Q_{H,n_J,HO}$ is the joint torque for the human-only (HO) simulation. C is the condition to be satisfied.

If either of those conditions are true, then, the motor and spring characteristics for task n_T and joint n_J are saved and the process moves on to the next joint. Then, if all joints have been optimized, the process goes to the next task until all tasks are done. If the condition on C or Q_{M,n_J} is false, then, the next motor characteristics will be used for the optimization until the conditions will be satisfied. If needed, stronger motors can be added manually to the list to satisfy the conditions. For this study, the condition C is chosen to be 0, which means lowering the user's torque to a maximum, i.e. 0 Nm.

The linear solver MUMPS from the IPOPT library was used with the three possible options of a threshold, a relative threshold, and a constraints violation threshold, which were all set at 1e-4 by default. The geometric optimizations took approximately 2 minutes for each functional task and 15 minutes for the combined optimization and the dynamic optimization took approximately 30 minutes (no-spring) to 2 hours (w-spring) on Windows 10, Intel® Core™ i7-7500U CPU @2.7 GHz.

3. Results

3.1 Geometrical optimization

Following the methodology presented in Section 2.4, we optimized the geometric dimensions $\boldsymbol{l}_E$ of the exoskeleton for the 6 functional tasks presented in Table 1. Figure 8A shows the norm of loop constraints $\boldsymbol{h}_l$. The red curves represent the non-optimized lengths that were approximately chosen with the 3D CAD software, while the black curves are the optimized lengths. The average of the optimized values is 2.9×10^{-5}, compared with the non-optimized value, 4.2×10^{-4}.

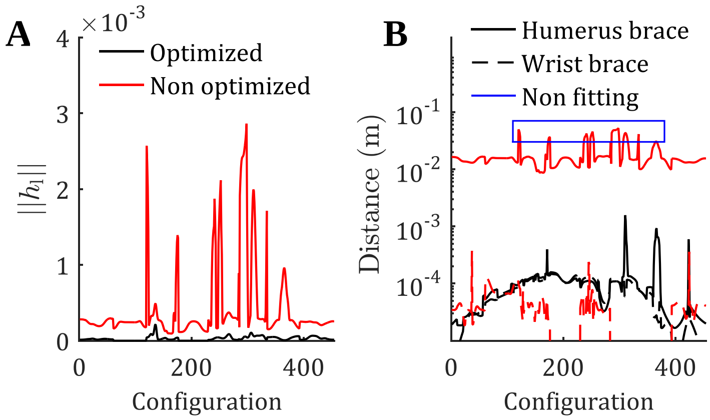

Figure 8. A. Norm of the loop constraints $\boldsymbol{h}_{loop}$ for the optimized and non-optimized lengths. B. Distance between the exoskeleton and the arm at the humerus brace point and wrist brace point for the optimized and non-optimized lengths.

Figure 8B presents the distance between the exoskeleton and the human arm at the humerus brace point and the wrist brace point. For the optimized lengths, the maximum distance is under 1 cm at both points. However, the humerus point distance for the non-optimized lengths is over 3 cm for 10.8% of the configurations, as shown in the blue box.

To evaluate the global distance between the exoskeleton and the arm around the shoulder, the summation part of Equation 6 was used for all configurations for d_{1-7}. The non-optimized total sum was 0.89 m compared to 1.02 m with optimized values. The distance between the exoskeleton and the arm, $l_{E,8}$ and $l_{E,9}$, went from 8.0 cm for the non-optimized lengths, to 7.1 cm with the optimized lengths.

3.2 Dynamic Synthesis

3.2.1 Backward recursive joint sizing

The following results were obtained with the dynamic optimization from Sections 2.5.1 to 2.5.3. The most distal motorized articulation is the forearm joint. Evaluating the OCP with motor HKX D101 reduced the user's joint torque to approximately zero, for the whole trajectory, as shown in Figure 9.

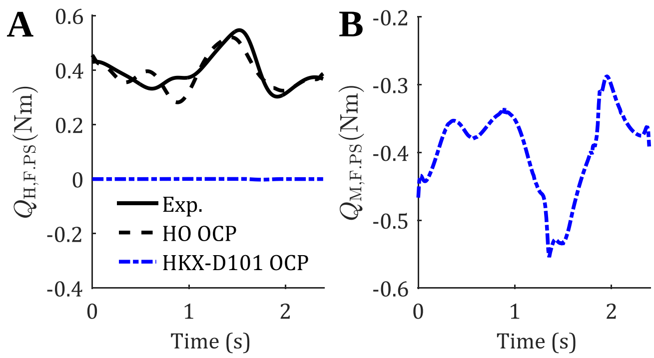

Figure 9. A. User's joint torque for the experimental data, HO OCP and with the HKX D101 motor. B. Exoskeleton joint torque for the PS movement.

At the elbow joint, Figure 10 presents the user's RMS joint torques in function of the exoskeleton RMS joint torque for each motor presented in Table 3 (Appendix A), with and without passive elements. The result for the spring only (SO) OCP is also shown. For each result, one can see that adding passive elements lowers the RMS user's joint torque by an average of 0.56 Nm, 23% of the HO OCP, when discarding the motors that reduce the torque to a minimum without passive elements. For the DMX XH540 DB motor, we can also see that without the passive element, it cannot lower the user's torque to a minimum, although is able to with the passive element. This is also highlighted in Figure 11A, where one can see a small segment where this motor is not at the minimum torque, while the version with the passive element is at the minimum torque.

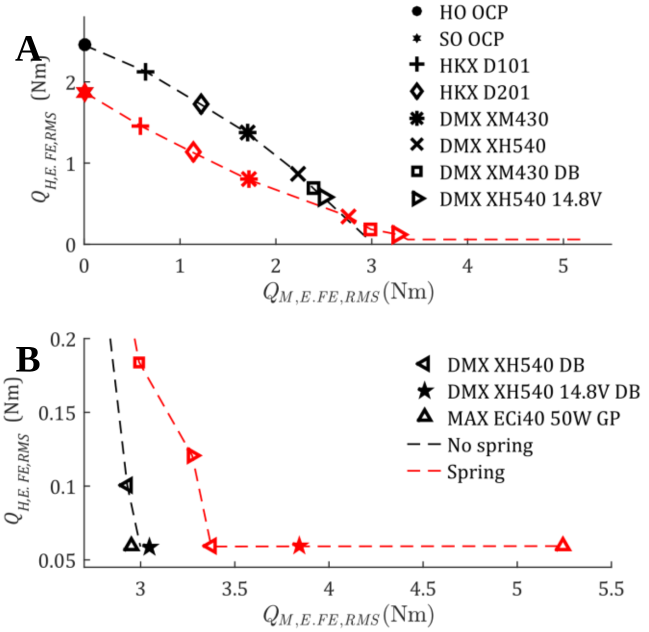

Figure 10. User's RMS elbow joint torques compared with exoskeleton RMS elbow joint torques for all the motors in tab X. A. Full graph. B. Close-up at the minimum user RMS torque. Lines are for visual aid, and are not related to additional data.

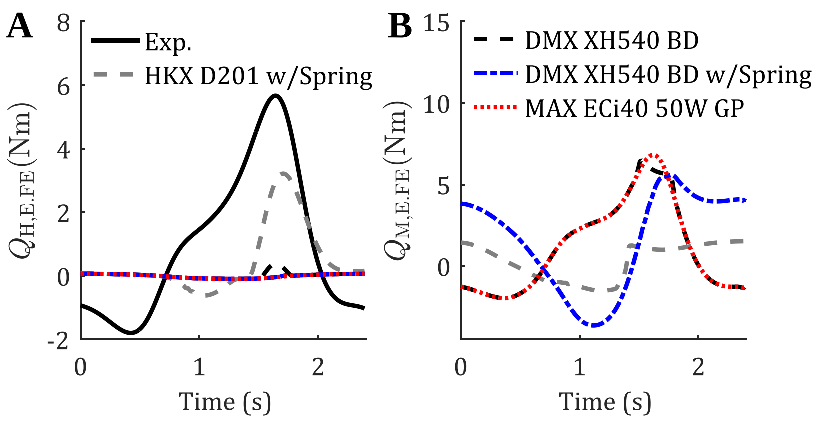

Figure 11. A. Human joint torque for the experimental data, HO OCP and several motors for the elbow flexion extension joint. B. Exoskeleton joint torques.

At the shoulder joint (Figure 12), adding passive elements lowers the RMS user's joint torque by an average of 3.31, 51% of the HO OCP, Nm for the *Eat with spoon* task and 3.06 Nm, 40% of the HO OCP, for the *Arm frontal reach* task. Both are evaluated with the DMX H540 DB at the elbow.

In Figure 12, to identify the impact on the shoulder joint of using a lighter or heavier motor at the elbow joint, a similar graph to the one of Figure 10 is presented for two functional tasks. *For* the *Eat with a spoon* task, in the simulation without passive elements, the use of the lighter motor at the elbow either reduces the user's joint torque for smaller motors or reduces the motor torque for stronger motors by an average of 0.33 Nm. For the simulation with passive elements, the average torque difference between the two motors is negligible (0.02 Nm). The same observation can be made for the *Arm frontal reach* task presented in where the reduction is 0.45 Nm without passive elements and 0.05 Nm with passive elements.

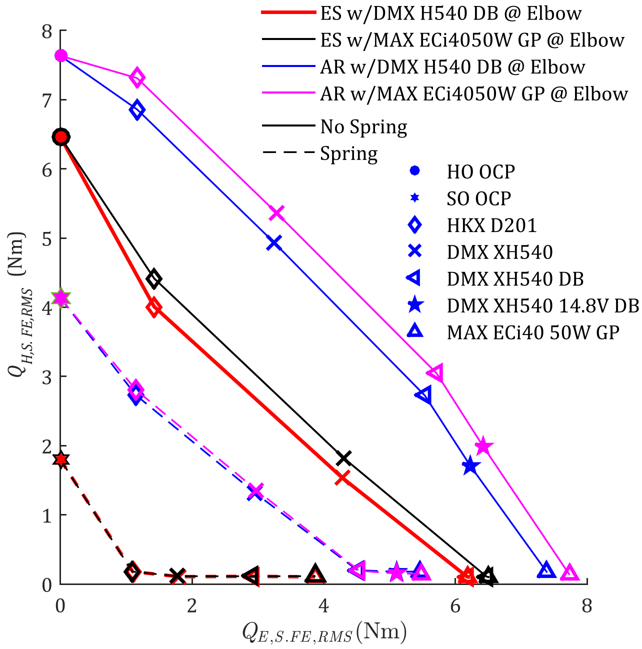

Figure 12. User RMS shoulder joint torques compared with the exoskeleton RMS shoulder joint torques for a selection of motors. Straight line are simulations without passive elements while dashed lines are with passive elements. Red and black lines are the *Eat with spoon* functional task with a lighter (DMX XH540 DB) and heavier motor (MAX ECi4050W GP) at the elbow joint respectively. Blue and purple lines are the *Arm frontal reach* functional task with a lighter (DMX XH540 DB) and heavier motor (MAX ECi4050W GP) at the elbow joint respectively. Lines are for visual aid and are not related to additional data.

3.2.2 Dynamic synthesis procedure

The result presented in Table 2 were obtained by the task-specific dynamic synthesis procedure shown in Figure 7 in Section 2.5.4. The user's joints RMS torques were reduced to less than 11% of the human-only RMS torques, $Q_{H,HO}$, for all tasks and joints except the S. AA joint in task RL which is reduced to 27.2%. Therefore, the condition

$C = 0$ was met for the F. PS joint and for all the other joints, the condition on the motor winding limit was met (see section 2.5.4).

Table 2. RMS user's joint torque Q_H, percentage of RMS user's joint torque without exoskeleton $Q_{H,HO}$, torsion spring stiffness k and torsion spring neutral position q_0 for each joint and each task. The results come from the dynamic synthesis procedure.

Joints	Value	Functional Task					
		ES	AR	RL	OD	CH	ZC
S. AA	Q_H [Nm]	0.1	0.2	0.7	0.2	0.1	0.1
	% of $Q_{H,HO}$	2.7	8.4	27.2	10.6	8.6	3.7
	k [Nm/rad]	4.5	17.8	16.3	4.7	18.6	18.2
	q_0 [rad]	1.4	0.7	0.7	2.0	0.4	0.6
	Motor	DMX XH540	DMX XH540	DMX XH540 DB	DMX XH540 DB	DMX XH540	DMX XH540
S. FE	Q_H [Nm]	0.1	0.2	0.2	0.1	0.1	0.1
	% of $Q_{H,HO}$	0.7	1.8	2.2	1.1	1.8	0.9
	k [Nm/rad]	6.6	3.3	3.8	2.8	2.8	3.9
	q_0 [rad]	0.1	1.5	0.9	0.8	1.1	0.1
	Motor	DMX XH540	DMX XH540 DB	DMX XH540 14.8V DB	DMX XH540 DB	DMX XH540 14.8V	DMX XH540 14.8V
E. FE	Q_H [Nm]	0.1	0.1	0.1	0.1	0.1	0.1
	% of $Q_{H,HO}$	2.3	2.1	3.2	1.9	3.8	2.6
	k [Nm/rad]	4.8	2.0	5.8	5.6	8.7	8.6
	q_0 [rad]	1.9	2.3	1.4	1.4	1.82	2.1
	Motor	DMX XH540 14.8V	DMX XH540 DB	DMX XH540 DB	DMX XH540 DB	DMX XH540 DB	DMX XH540 14.8V
F. PS	Q_H [Nm]	~0.00	~0.00	~0.00	~0.00	~0.00	~0.00
	% of $Q_{H,HO}$	~0.00	~0.00	~0.00	~0.00	~0.00	~0.00
	Motor	HKX D101	HKX D101	HKX D101	HKX D101	HKX D101	HKX D101

4. Discussion

The global objective of this study was to develop a procedure for geometric and dynamic synthesis of assistive upper limb exoskeletons, to serve as a tool to support their design. These exoskeletons should reduce the effort required by the user during functional tasks (dynamic consideration) and should fit the size of the user (geometric consideration). The results are discussed in descending order of importance: Section 4.1 discusses the complete dynamic synthesis procedure, then Section 4.2 discusses the dynamic optimization results, and Section 4.3 discusses the geometric optimization.

4.1 Dynamic synthesis procedure

The dynamic synthesis procedure and tools summarized in Figure 7 were developed for an assistive passive and active upper limb exoskeleton for six functional tasks. The main results of this procedure are reported in Table 2, which presents the selection of motors, the results for the passive element characteristics k and q_0, the user's torque Q_H, in the assisted joint and the reduction percentage of the user's torque compared with the human-only simulations, % of $Q_{H,HO}$, for all joints during each functional task. This is a task-specific procedure to design the exoskeleton for one task and for one user. This type of design could be interesting in a work environment where a complex task is carried out repeatedly such as wall painting or in the assistive medical field for a specific task such as eating.

The results in Table 2 could be used in a more generalized approach. For instance, by selecting the largest motor for each joint across all the functional tasks, the exoskeleton would have the capacity to perform each task if the spring characteristics are switched between tasks. This could be done by the user with a clutch mechanism or simply by changing the spring directly. Additionally, optimizing the spring selection could limit the number of required springs. From a practical perspective, in a work environment where workers carry out multiple tasks in the manufacturing chain, such an exoskeleton could allow the employer to acquire one general exoskeleton instead of multiple task-specific exoskeletons.

To evaluate the dynamic performance of the developed procedure, the user's joint torques results presented in Table 2 were analyzed. For the F. PS joint, user's torque could be reduced to near 0 Nm and is the only joint where the condition $C = 0$ could be met. For the other joints, the condition on the motor winding was met (Section 2.5.4). The E. FE user's torque, Q_H, represents less than 5% of the human-only simulation torque, $Q_{H,HO}$, and 2% for the S. FE in all functional tasks. The last motorized joint torque, S. AA, could be reduced to less than 10.6% for five out of the six tasks. This still represents a significative reduction of effort for the user. For the *Arm frontal reach Left to Right* task, the resulting torque is still 27.2% of the human-only simulation.

For each motor that could not reach a *user torque ratio,* $C = 0$, it suggests that the motor axis is not correctly aligned with the user's joint rotation axis. These misalignments could cause parasitic torques in the user's joints that can eventually result in injuries. This is a well-known problem in exoskeleton design and has been discussed in many studies [21, 46]. Those parasitic torques and forces should be measured and minimized in the dynamic optimisation. A limitation of this work is that, as this problem is greatly linked to geometric parameters, a combination of both geometric and dynamic optimisations is required to reduce effectively the parasite torques. However, this was not implemented and could be investigated further in future works.

In this study, the *user torque ratio,* C was chosen to be 0 for illustration. This implied that the user did not need to produce torque to use the exoskeleton. But a low user's joint torque is related to low muscle forces around this joint, which can be associated to muscular atrophy [47]. Studies should be pursued to evaluate the longer-term effect of wearing such exoskeletons where the user does not need to produce torque, and to determine a safe *user torque ratio* for the different purposes, such as workplace or medical assistance. Moreover, this study was limited to the evaluation of the user's joint torque, but a more biofidel evaluation of the user's effort are the muscle forces [36, 48, 49]. Then, a safe *user muscle force ratio* should also be evaluated through further studies.

4.2 Dynamic optimization

Figures 10 and 12 present a comparison between the user's RMS elbow joint torques and the exoskeleton RMS elbow joint torques. The reduction of the user's torque by adding passive elements is significative, with an average of 0.56 and 3.31 Nm for the *Eat with a spoon* task at the elbow and shoulder joints, respectively, while the average for the *Arm frontal reach* task at the shoulder joint is 3.06 Nm. This allowed the use of weaker motors in the three cases, enabling to globally reduce the torque required by the exoskeleton motors. This was true for all joints, except the F. PS. As shown in Figure 9 and Table 2, the HKX D101 motor could reduce the user's torques to 0 Nm without the use of passive elements. Springs are not relevant for this joint, as it is mostly in the horizontal plane and is, therefore, less affected by gravity.

Figure 12 also enables to compare the effects on the shoulder, between the use of a lighter or heavier motor at the elbow joint. For the *Eat with spoon* task and *Arm frontal reach* task the difference of using lighter or heavier motor is 0.33 Nm and 0.45 Nm without passive elements and negligible values with passive elements, respectively 0.02 Nm and 0.05 Nm. This suggest that the passive elements can reduce the dependencies between joints. Indeed, the springs compensate the static effect, i.e. gravity effect of the heavier motor. The small differences, 0.02 Nm and 0.05 Nm are due to the increased inertia of the motors. This can be interesting if the exoskeleton is to be designed for low dynamic tasks, the passive elements could enable the use of bigger motors in distal joint such as the F. PS and E. FE without requiring bigger motors at the proximal joints S. FE and S. AA. In future studies, a sensitivity analysis on the level of dynamics and size of motors could be conducted to identify the limits of the previous statement. Moreover, adding bigger motors would globally add weight to the exoskeleton, and the effect on the back and lower limbs should be considered.

Figure 11A shows the impact of the spring for motor DMX H540 DB torque trajectory as the simulation with black dashed line, the no-spring simulation, cannot lower the torque to the minimum while the blue curve, the with-spring simulation, is at the minimum. This enabled to use this motor instead of the heavier MAX ECi40 50W GP. However, in Figure 11B, for the two motors (red and blue) that could reduce the user's joint torque to the minimum value, the torque curves differ largely because of the spring element. Therefore, the control strategy of the exoskeleton will require to take this in consideration.

4.3 Geometric optimization

The objective of the geometric optimization was to minimize the loop constraints $\boldsymbol{h}_l$ while avoiding collisions with the human. This was done for all functional tasks simultaneously resulting in a fully sized exoskeleton.

Figure 8A shows a reduction of the loop constraints norm $\|\boldsymbol{h}_l\|$ by an average factor of 14.6 when the lengths of the exoskeleton segments are optimized. This reduction yields, as seen in Figure 8B, a distance of less than 1 cm for all configurations in all functional tasks between the exoskeleton braces and the arm and forearm connection points. With the non-optimized lengths, 10.8% of the configuration had a difference of more than 3 cm at the arm connection point, as is presented by the blue box in Figure 8B. With the human arm skin movement that can vary greatly [50] and the adjustments on the user, it can be assumed that distances of less than 3 cm could still fit the user. Therefore, the gain of this optimization compared with the non-optimized lengths is 11%. This is important to guarantee the fit of the exoskeleton to the user without collision with his body.

Another result is the sum of distance d_{1-7}, initially presented in Figure 5, which evaluates the distance between the exoskeleton and the shoulder complex. The total for the non-optimized lengths, 0.89 m, was lower than the total for the optimized lengths, 1.02 m. The distances between the exoskeleton and the user's arm, $l_{E,8}$ and $l_{E,9}$, initially presented in Figure 4, went from 8 cm to 7.1 cm, globally bringing the exoskeleton closer to the body, thus reducing the overall size of the system. However, the most interesting element of this geometric optimization is the automatization of the process to personalize exoskeletons faster than a visual identification or trial and error for different users.

5. Conclusion

This objective of the work presented in this study was to develop geometric and dynamic synthesis procedure to design and personalize a 3D assistive passive and active upper limb exoskeletons. This was applied to six specific functional tasks of one healthy subject. To do so, sub-objectives were, first, to find the exoskeleton size to fit the user for all functional tasks and, secondly, to find the motor selection and passive element characteristics to reduce the user effort to a minimum for each task.

Consequently, successful geometric and dynamic synthesis procedures were developed and applied to 6 functional tasks following a wide range of motion:

First, for the geometric optimization, a framework was built through a non-linear problem minimizing the loop closure constraints between the exoskeleton and the arm for all the functional tasks configurations. The output of this framework was the dimensions of the exoskeleton. The constraints were reduced by a factor 14.6, which resulted in a gain of 10.8% of closed configurations compared with a visual identification on the CAD model of the exoskeleton.

Secondly, for the dynamic optimization, a framework was built through an optimal control problem using the human position, velocities, and torques as well as exoskeleton torques and passive elements characteristics as variables. The goal was to reduce the user's joint torques to a minimum, while respecting the winding limits of the motors. The dynamic synthesis enabled to identify the characteristics of the motors and passive elements for all the functional tasks. Moreover, the user's joint torques could be lowered to 10.6% off of the human-only torques for all joints and tasks except for the S. AA joint in one task that stayed at 27.2%. These residual torques were caused by misalignment with the human joints, resulting in eventual parasitic torques that could harm the user. The dynamic optimization procedure also showed the importance of using passive elements in the E. FE, S. FE and S. AA joints as they could help the motors to reduce the user's joint torques. For instance, the spring reduced the S. FE joint torque by an average of 3.31 Nm for the *Eat with a spoon task*. This resulted in the selection of a smaller and lighter motor to compensate the user's effort at the shoulder.

Future works could be performed to further improve the developed procedures. Some possible avenues are as follows: First, the geometric and dynamic optimization could be combined to take care of the misalignment problem, as it is related to the geometric parameters. The parasitic torques could then be minimized. Secondly, the user muscle force could be minimized instead of the joint torque for a more anatomically and physiologically realistic reduction of the user effort by using the methods proposed in [49, 51]. Thirdly, one could find the safe *user muscle force ratio* that will not cause muscular atrophy when using the exoskeletons for long-term periods. Finally, a sensitive study could be carried out to characterize how the different geometric and dynamic parameters co-influence each other.

References

1. Gopura, R.A.R.C., Bandara, D.S.V., Kiguchi, K., Mann, G.K.I.: Developments in hardware systems of active upper-limb exoskeleton robots: A review. Robotics and Autonomous Systems. 75, 203–220 (2016). https://doi.org/10.1016/j.robot.2015.10.001
2. Koo, D., Chang, P.H., Sohn, M.K., Shin, J.: Shoulder mechanism design of an exoskeleton robot for stroke patient rehabilitation. In: 2011 IEEE International Conference on Rehabilitation Robotics. pp. 1–6 (2011)
3. Frisoli, A., Rocchi, F., Marcheschi, S., Dettori, A., Salsedo, F., Bergamasco, M.: A new force-feedback arm exoskeleton for haptic interaction in virtual environments. In: First Joint Eurohaptics Conference and Symposium on Haptic Interfaces for Virtual Environment and Teleoperator Systems. World Haptics Conference. pp. 195–201 (2005)
4. Bartolo, M., De Nunzio, A.M., Sebastiano, F., Spicciato, F., Tortola, P., Nilsson, J., Pierelli, F.: Arm weight support training improves functional motor outcome and movement smoothness after stroke. Funct Neurol. 29, 15–21 (2014)
5. Marcheschi, S., Salsedo, F., Fontana, M., Bergamasco, M.: Body Extender: Whole body exoskeleton for human power augmentation. In: 2011 IEEE International Conference on Robotics and Automation. pp. 611–616 (2011)
6. Bougrinat, Y., Achiche, S., Raison, M.: Design and development of a lightweight ankle exoskeleton for human walking augmentation. Mechatronics. 64, 102297 (2019). https://doi.org/10.1016/j.mechatronics.2019.102297
7. Zoss, A., Kazerooni, H.: Design of an electrically actuated lower extremity exoskeleton. Advanced Robotics. 20, 967–988 (2006). https://doi.org/10.1163/156855306778394030
8. Huysamen, K., Bosch, T., de Looze, M., Stadler, K.S., Graf, E., O'Sullivan, L.W.: Evaluation of a passive exoskeleton for static upper limb activities. Applied Ergonomics. 70, 148–155 (2018). https://doi.org/10.1016/j.apergo.2018.02.009
9. Gunn, M., Shank, T.M., Eppes, M., Hossain, J., Rahman, T.: User Evaluation of a Dynamic Arm Orthosis for People With Neuromuscular Disorders. IEEE Transactions on Neural Systems and Rehabilitation Engineering. 24, 1277–1283 (2016). https://doi.org/10.1109/TNSRE.2015.2492860
10. Font-Llagunes, J.M., Lugrís, U., Clos, D., Alonso, F.J., Cuadrado, J.: Design, Control, and Pilot Study of a Lightweight and Modular Robotic Exoskeleton for Walking Assistance After Spinal Cord Injury. J. Mechanisms Robotics. 12, (2020). https://doi.org/10.1115/1.4045510
11. Young, A.J., Ferris, D.P.: State of the Art and Future Directions for Lower Limb Robotic Exoskeletons. IEEE Trans Neural Syst Rehabil Eng. 25, 171–182 (2017). https://doi.org/10.1109/TNSRE.2016.2521160
12. Yan, T., Cempini, M., Oddo, C.M., Vitiello, N.: Review of assistive strategies in powered lower-limb orthoses and exoskeletons. Robotics and Autonomous Systems. 64, 120–136 (2015). https://doi.org/10.1016/j.robot.2014.09.032
13. Maciejasz, P., Eschweiler, J., Gerlach-Hahn, K., Jansen-Troy, A., Leonhardt, S.: A survey on robotic devices for upper limb rehabilitation. Journal of NeuroEngineering and Rehabilitation. 11, 3 (2014). https://doi.org/10.1186/1743-0003-11-3
14. Haumont, T., Rahman, T., Sample, W., M. King, M., Church, C., Henley, J., Jayakumar, S.: Wilmington Robotic Exoskeleton: A Novel Device to Maintain

Arm Improvement in Muscular Disease. Journal of Pediatric Orthopaedics. 31, e44 (2011). https://doi.org/10.1097/BPO.0b013e31821f50b5
15. Altenburger, R., Scherly, D., Stadler, K.S.: Design of a passive, iso-elastic upper limb exoskeleton for gravity compensation. Robomech J. 3, 12 (2016). https://doi.org/10.1186/s40648-016-0051-5
16. Shank, T., Eppes, M., Hossain, J., Gunn, M., Rahman, T.: Outcome Measures with COPM of Children using a Wilmington Robotic Exoskeleton. The Open Journal of Occupational Therapy. 5, (2017). https://doi.org/10.15453/2168-6408.1262
17. Elliott, G., Sawicki, G.S., Marecki, A., Herr, H.: The biomechanics and energetics of human running using an elastic knee exoskeleton. In: 2013 IEEE 13th International Conference on Rehabilitation Robotics (ICORR). pp. 1–6 (2013)
18. Perez Luque, E.: Evaluation of the Use of Exoskeletons in the Range of Motion of Workers. (2019)
19. Matthew, R.P., Mica, E.J., Meinhold, W., Loeza, J.A., Tomizuka, M., Bajcsy, R.: Introduction and initial exploration of an Active/Passive Exoskeleton framework for portable assistance. In: 2015 IEEE/RSJ International Conference on Intelligent Robots and Systems (IROS). pp. 5351–5356 (2015)
20. Smith, R.L., Lobo-Prat, J., van der Kooij, H., Stienen, A.H.A.: Design of a perfect balance system for active upper-extremity exoskeletons. In: 2013 IEEE 13th International Conference on Rehabilitation Robotics (ICORR). pp. 1–6 (2013)
21. Galinski, D., Sapin, J., Dehez, B.: Optimal design of an alignment-free two-DOF rehabilitation robot for the shoulder complex. In: 2013 IEEE 13th International Conference on Rehabilitation Robotics (ICORR). pp. 1–7 (2013)
22. Sarac, M., Solazzi, M., Sotgiu, E., Bergamasco, M., Frisoli, A.: Design and kinematic optimization of a novel underactuated robotic hand exoskeleton. Meccanica. 52, 749–761 (2017). https://doi.org/10.1007/s11012-016-0530-z
23. Hayashi, Y., Dubey, R., Kiguchi, K.: Torque optimization for a 7DOF upper-limb power-assist exoskeleton robot. In: 2011 IEEE Workshop on Robotic Intelligence In Informationally Structured Space. pp. 49–54 (2011)
24. Aoustin, Y., Formalskii, A.M.: Walking of biped with passive exoskeleton: evaluation of energy consumption. Multibody Syst Dyn. 43, 71–96 (2018). https://doi.org/10.1007/s11044-017-9602-7
25. Zhou, L., Li, Y., Bai, S.: A human-centered design optimization approach for robotic exoskeletons through biomechanical simulation. Robotics and Autonomous Systems. 91, 337–347 (2017). https://doi.org/10.1016/j.robot.2016.12.012
26. Manns, P., Sreenivasa, M., Millard, M., Mombaur, K.: Motion Optimization and Parameter Identification for a Human and Lower Back Exoskeleton Model. IEEE Robotics and Automation Letters. 2, 1564–1570 (2017). https://doi.org/10.1109/LRA.2017.2676355
27. Laitenberger, M., Raison, M., Périé, D., Begon, M.: Refinement of the upper limb joint kinematics and dynamics using a subject-specific closed-loop forearm model. Multibody Syst Dyn. 33, 413–438 (2015). https://doi.org/10.1007/s11044-014-9421-z
28. Ehrig, R.M., Taylor, W.R., Duda, G.N., Heller, M.O.: A survey of formal methods for determining the centre of rotation of ball joints. Journal of Biomechanics. 39, 2798–2809 (2006). https://doi.org/10.1016/j.jbiomech.2005.10.002

29. Ehrig, R.M., Taylor, W.R., Duda, G.N., Heller, M.O.: A survey of formal methods for determining functional joint axes. Journal of Biomechanics. 40, 2150–2157 (2007). https://doi.org/10.1016/j.jbiomech.2006.10.026
30. Automatic Joint Parameter Estimation from Magnetic Motion Capture Data, http://graphics.berkeley.edu/papers/Obrien-AJP-2000-05
31. Yeadon, M.R.: The simulation of aerial movement—II. A mathematical inertia model of the human body. Journal of Biomechanics. 23, 67–74 (1990). https://doi.org/10.1016/0021-9290(90)90370-I
32. Lecours, S.: Développement d'un exosquelette portable motorisé des membres supérieurs pour les enfants atteints de troubles neuromusculaires, https://publications.polymtl.ca/4048/, (2019)
33. Samin, J.-C., Fisette, P.: Symbolic Modeling of Multibody Systems. Springer Netherlands (2003)
34. Docquier, N., Poncelet, A., Fisette, P.: ROBOTRAN: a powerful symbolic gnerator of multibody models. Mechanical Sciences. 4, 199–219 (2013). https://doi.org/10.5194/ms-4-199-2013
35. Rosen, J., Perry, J.C., Manning, N., Burns, S., Hannaford, B.: The human arm kinematics and dynamics during daily activities - toward a 7 DOF upper limb powered exoskeleton. In: ICAR '05. Proceedings., 12th International Conference on Advanced Robotics, 2005. pp. 532–539 (2005)
36. Raison, M.: On the quantification of joint and muscle efforts in the human body during motion, https://dial.uclouvain.be/pr/boreal/object/boreal:22741, (2009)
37. Collard, J.-F.: Geometrical and kinematic optimization of closed-loop multibody systems/Optimisation géométrique et cinématique de systèmes multicorps avec boucles cinématiques, https://dial.uclouvain.be/pr/boreal/object/boreal:5212, (2007)
38. Galinski, D.: Conception et optimisation d'un robot de rééducation neuromotrice du membre supérieur avec compensation active de la gravité, https://dial.uclouvain.be/pr/boreal/object/boreal:153440, (2014)
39. Bell, M.L., Sargent, R.W.H.: Optimal control of inequality constrained DAE systems. Computers & Chemical Engineering. 24, 2385–2404 (2000). https://doi.org/10.1016/S0098-1354(00)00566-4
40. Fabien, B.C.: Numerical solution of constrained optimal control problems with parameters. Applied Mathematics and Computation. 80, 43–62 (1996). https://doi.org/10.1016/0096-3003(95)00280-4
41. von Stryk, O.: Numerical Solution of Optimal Control Problems by Direct Collocation. In: Bulirsch, R., Miele, A., Stoer, J., and Well, K. (eds.) Optimal Control: Calculus of Variations, Optimal Control Theory and Numerical Methods. pp. 129–143. Birkhäuser, Basel (1993)
42. Andersson, J.A.E., Rawlings, J.B.: Sensitivity Analysis for Nonlinear Programming in CasADi∗∗The authors would like to thank Johnson Controls International Inc, for generous support that has made this work possible. IFAC-PapersOnLine. 51, 331–336 (2018). https://doi.org/10.1016/j.ifacol.2018.11.055
43. Diehl, M., Gros, S.: Numerical Optimal Control (preliminary and incomplete draft). 357
44. Gros, S.: Numerical Optimal Control with DAEs Lecture 12: Optimal Control with DAEs, https://www.syscop.de/files/2015ws/noc-dae/lecture%20slides/12-DAEOptimalControl.pdf
45. Petuskey, K., Bagley, A., Abdala, E., James, M.A., Rab, G.: Upper extremity kinematics during functional activities: Three-dimensional studies in a normal

pediatric population. Gait & Posture. 25, 573–579 (2007). https://doi.org/10.1016/j.gaitpost.2006.06.006
46. Näf, M.B., Junius, K., Rossini, M., Rodriguez-Guerrero, C., Vanderborght, B., Lefeber, D.: Misalignment Compensation for Full Human-Exoskeleton Kinematic Compatibility: State of the Art and Evaluation. Appl. Mech. Rev. 70, (2018). https://doi.org/10.1115/1.4042523
47. Thomas, C.K., Zaidner, E.Y., Calancie, B., Broton, J.G., Bigland-Ritchie, B.R.: Muscle Weakness, Paralysis, and Atrophy after Human Cervical Spinal Cord Injury. Experimental Neurology. 148, 414–423 (1997). https://doi.org/10.1006/exnr.1997.6690
48. Crowninshield, R.D., Brand, R.A.: A physiologically based criterion of muscle force prediction in locomotion. Journal of Biomechanics. 14, 793–801 (1981). https://doi.org/10.1016/0021-9290(81)90035-X
49. Wen, J., Raison, M., Achiche, S.: Using a cost function based on kinematics and electromyographic data to quantify muscle forces. Journal of Biomechanics. 80, 151–158 (2018). https://doi.org/10.1016/j.jbiomech.2018.09.002
50. Mahmud, J., Holt, C.A., Evans, S.L.: An innovative application of a small-scale motion analysis technique to quantify human skin deformation in vivo. Journal of Biomechanics. 43, 1002–1006 (2010). https://doi.org/10.1016/j.jbiomech.2009.11.009
51. Raison, M., Detrembleur, C., Fisette, P., Samin, J.-C.: Assessment of Antagonistic Muscle Forces During Forearm Flexion/Extension. In: Arczewski, K., Blajer, W., Fraczek, J., and Wojtyra, M. (eds.) Multibody Dynamics: Computational Methods and Applications. pp. 215–238. Springer Netherlands, Dordrecht (2011)

Appendix A: Motor parameters

Table 3. Motor parameters.

Motors (Abbreviation)	Voltage (V)	Max torque (Nm)	Cont. torque (Nm)	Cont. speed (rad/s)	Mass (kg)
Herkulex DRS-101 (HKX D101)	12	0.8	0.17	6.3	0.05
Herkulex DRS-201 (HKX D201)	12	1.6	0.22	7.1	0.06
Dynamixel XM430 210W (DMX XM430)	12	2.4	0.00	9.9	0.08
Dynamixel XM430 210W x2 (DMX 430 DB)	12	4.8	0.00	9.9	0.16
Dynamixel XM540 150W (DMX XH540/ DMX XH540 14.8V)	12 14.8	4.7 5.6	0.00 0.00	7.3 8.9	0.17 0.17
Dynamixel XM540 150W x2 (DMX XH540 DB/ DMX XH540 14.8V DB)	12 14.8	9.4 11.2	0.00 0.00	7.3 8.9	0.33 0.33
Maxon ECi40 50W w/ Maxon Gearhead GP42 15Nm (MAX ECi4050W GP)	24	9.4	1.01	187	0.54

Appendix B: Optimal control problem evaluation

Unless otherwise indicated, the following results were obtained with the *Eat with spoon* functional task to illustrate the process for one movement. The first step was to valid the kinematics and dynamics obtained with a human-only OCP following the method proposed in sections 2.5.1 to 2.5.3. These results are presented in Figure 13: sub-Figures 13A-D shows that the kinematics of the movement was respected, while sub-Figures 13E-F show a reduction of the RMS human joint torque by 3% for the elbow joint and 5% for the shoulder joint.

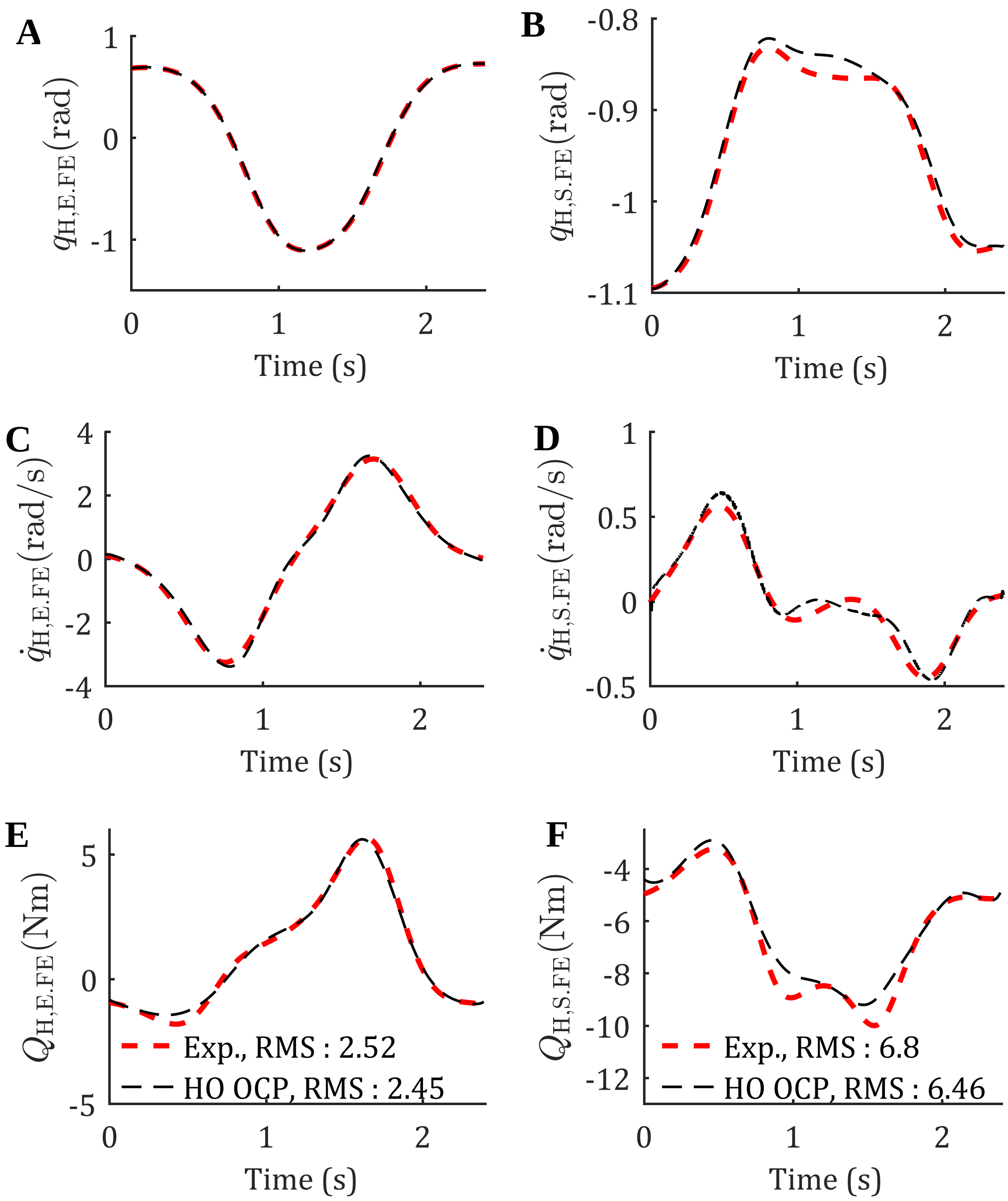

Figure 13. Experimental data and human only (HO) optimal control problem (OCP), A and B, position, C and D, velocities, E and F, joint torques and RMS torques.

Figure 13 enables to validate the kinematics and dynamics obtained with the OCP. In Figures 13A-D the kinematics were respected thus keeping a valid human trajectory. This is important, especially for a task such as eating, where the orientation of the hand is crucial. The small differences in kinematics are reflected in the dynamics by Figures 13E-F, where there is a slight reduction of the human joint torque with the OCP suggesting the solver changed the trajectory to minimize the joint torques. This fits the cost function described by Equation 17.